VOLUME 7, NUMBER 5, MAY 2007

NANO LETTERS

Highly Tunable Infrared Extinction Properties of Gold Nanocrescents

Rostislav Bukasov and Jennifer S. Shumaker-Parry*

Department of Chemistry, 315 South 1400 East, Room 2020, University of Utah, Salt Lake City, Utah 84112-0850

Received October 2, 2006; Revised Manuscript Received February 13, 2007

ABSTRACT

The infrared extinction properties of gold nanocrescents fabricated using nanosphere template lithography were studied. The nanocrescents exhibit multiple, structurally tunable localized surface plasmon resonances (LSPRs) across a broad spectral range (560–3600 nm). Plasmon resonances in the infrared have large extinction efficiencies of ~20 and peaks as narrow as 0.07 eV. The nanocrescents also have high refractive index sensitivities (370–880 nm/RIU) that are proportional to the LSPR wavelengths. The sensing figure of merit measured for ensembles of nanocrescents is as high as 2.4 for near-infrared plasmon resonances.

The possibility of tuning the unique optical properties of noble metal nanoparticles (MNPs) through control of structure and interparticle distances has motivated research efforts in developing new methods of nanoparticle design and assembly. For MNPs, the confined conduction electrons are induced to oscillate collectively when exposed to light of a proper resonance wavelength, leading to a localized surface plasmon resonance (LSPR). The LSPR phenomena include wavelength-selective photon absorption, emission, and scattering as well as the generation of locally amplified electromagnetic fields. These optical properties depend on and can be tuned by variations in the MNP's size,[1] shape,[2] composition,[3] interparticle distance,[4] and dielectric environment.[5]

The increasing diversity of MNPs reported in the literature is well matched by numerous prospective applications of LSPR-active particles as components in micro- and nanoscale optical devices,[6] substrates for surface-enhanced spectroscopies,[7–9] apertureless near-field microscopy probes,[10] chemical and biological sensors,[11] and as nonbleaching optical labels.[12] The typical red-shift of LSPR wavelengths due to an effective refractive index increase caused by binding of biomolecules to functionalized MNPs or a decrease of the average interparticle distance leading to LSPR coupling has been exploited in transmission-localized surface plasmon resonance (T-LSPR) spectroscopy,[13] assays based on MNP agglomeration,[14,15] molecular force rulers,[16] and chemical and biological sensors.[17] In addition to the LSPR sensitivity, highly localized electromagnetic fields produced at the sharp edges or tips of some nanostructures or between two coupled MNPs also play an important role in the application of MNPs. For example, localized electromagnetic field enhancements are important in surface-enhanced Raman scattering spectroscopy (SERS).[18–20]

One challenge associated with MNPs is the need to be able to tune the nanoparticles' optical properties for each specific application. For example, Van Duyne and co-workers

* Corresponding author. E-mail: shumaker-parry@chem.utah.edu.

10.1021/nl062317o CCC: $37.00
Published on Web 04/14/2007

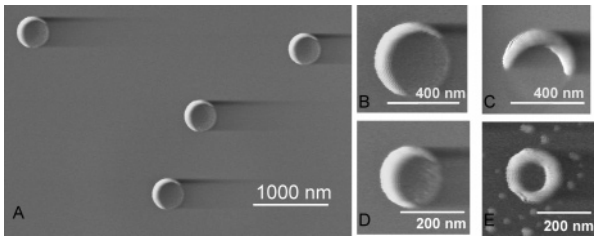

Figure 1. SEM images of nanocrescents templated with PS beads with diameters of (A−C) 356 nm, (D) 194 nm beads, and (E) nanorings templated with 125 nm diameter PS beads. Azimuthal angles of (A) 10° and (B) 55° with respect to the gold deposition source were used to produce different aspect ratios.

showed a significant affect of tuning the excitation wavelength relative to the LSPR wavelength for optimal enhancements and signal generation in SERS[4,21] and surface-enhanced infrared absorption spectroscopy (SEIRAS).[22] They showed that signals are most enhanced when the extinction maxima of MNPs or metal islands coincide with the excitation/emission spectral bands of the light source and the vibrational bands of the molecules of interest located in close proximity to the nanoparticles. In addition, control of the magnitude and the extent of localization of electromagnetic field enhancements also is critical for optimizing signals in surface-enhanced spectroscopies[20] or to produce microscopy probes with well-controlled and optimized spatial resolution.[10]

In this report, we present the highly sensitive, broadly tunable LSPR properties of crescent-shaped MNPs. The nanocrescents exhibit multiple, structurally tunable localized surface plasmon resonances (LSPR) from the visible to the infrared and are expected to behave as optical antennas due to their sharp structural features. The nanocrescents have been fabricated using nanosphere template lithography (NTL), an extension of nanosphere lithography (NSL).[23,24] Rather than using large numbers of close-packed spheres as in NSL, NTL uses individual nanopsheres as templates.[25−27] The NTL fabrication process for the nanocrescents combines nanosphere templating with angle-controlled metal film deposition and ion beam milling.[28,29] Polystyrene spheres (PS) with diameters ranging from 125 to 659 nm were used as templates. The SEM image in Figure 1A shows the ability to produce a large number of nanocrescents with well-defined and uniform size, shape, and orientation on a glass substrate using NTL.

The NTL technique is versatile, providing control of numerous structural features by controlling fabrication parameters. The template diameter and the gold film thickness determine the size and thickness, respectively, of the nanocrescents. Using the same diameter PS template, the sharpness of the nanocrescent tips and the distance between the tips can be changed by varying the gold film thickness and the incident deposition angles (i.e., the tilt angle with respect to the substrate surface normal and the incident angle with respect to the metal source). The effect of changing the metal film thickness and the deposition angles is shown in Figure 1B−F. In addition, by controlling the azimuthal angle with respect to the surface normal of the substrate the gap between the tips of the crescents can be incrementally decreased until there is no opening in the structure and continuous gold rings are formed.[29] Rings also may be fabricated using small templates (e.g., PS with diameters <125 nm) and low deposition angles to produce low aspect ratio structures, (i.e., the ratio of particle length to particle width or height) if the gold film thickness is approximately equal to or greater than $^1/_3$ of the template diameter (e.g., 45 nm for 125 nm diameter PS). The rings are the most symmetric if the azimuthal and deposition angles are minimal, 0° and 20°, respectively. This correlates with a previously published nanoring fabrication method.[28] Small islands surrounding the nanorings shown in Figure 1D are due to incomplete etching of the gold film. Ideally, etching parameters are adjusted so there are no islands remaining on the surface, as shown by SEM imaging. However, it is not trivial to adjust the etching time so that all traces of gold are removed from the surrounding surface without heating the substrate and melting the polystyrene colloid templates. Experimentally, we have found that the presence of small, thin islands (i.e., less than 10 nm wide and a few nanometers high as characterized by SEM and AFM) has no effect on the measured optical properties of the templated structures.

For all nanocrescents, the tips become sharper with an increase in the in-plane aspect ratio (i.e., ratio of length to width or length to height) due to an increase in the incident deposition angle or a decrease in gold thickness. The nanocrescents' thickness and the radius of curvature of the tips were characterized by AFM (data not shown) and SEM, respectively. The tip radius of curvature is less than 10 nm for the particles shown in the SEM images in Figure 1A,B,D.

The nanocrescents' optical properties were characterized by UV−visible−NIR extinction spectroscopy. The loss of light measured is due to scattering and absorption of incident light by the nanocrescents. The incident light is approximately 80% plane-polarized. The electric field polarization is parallel to the nanocrescent long axis for the data shown in Figures 2 and 3. Detailed polarization-dependent studies using a broad wavelength range polarizer to increase the extent of polarization are underway.

The spectra in Figure 2A and the data presented Table 1 are representative for nanocrescents produced using 125, 194, 356, and 465 nm diameter PS templates. At least three distinct peaks are shown in each spectrum. These peaks are easily resolved due to the uniform size, shape, and orientation of the nanocrescents, even for large-area (i.e., beam size 20 mm^2) ensemble measurements. For all of the nanocrescents, the shortest wavelength peak is observed at 600 ± 50 nm and is likely due to an out-of-plane resonance. Generally, the LSPR peak in the visible region has a small amplitude compared to the other LSPR peaks and is much less sensitive to the polarization of the incident light with respect to the orientation of the nanocrescents.

In addition to the peak in the visible region, nanocrescents exhibit at least two other longer wavelength peaks, as shown in Figure 2. The longitudinal plasmon resonance peak (e.g., the peak at 2470 nm for 356 nm diameter nanocrescents) dominates the spectrum when the incoming light is polarized along the crescent's long axis. The amplitude of the

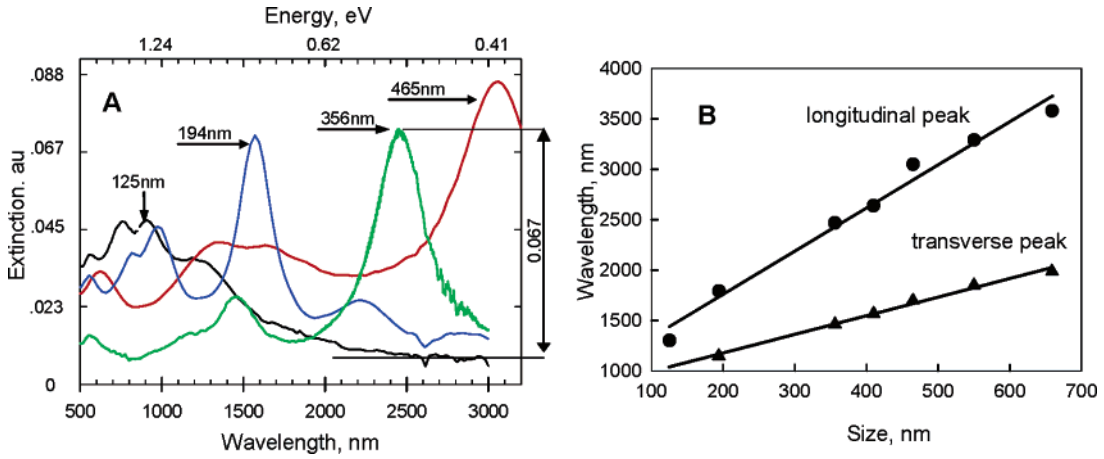

Figure 2. Size-dependent nanocrescent LSPR properties. (A) Ensemble extinction spectra with the PS bead template diameter shown near the longitudinal peaks. The extinction value (0.067) for 356 nm template diameter nanocrescents was found from the difference between the baseline established by a Lorentzian peak fit and the peak maximum. (B) The linear dependence of nanocrescent LSPR peaks on the diameter of the PS template used to fabricate the nanocrescents. R^2 values for longitudinal and transverse resonances are 0.982 and 0.993, respectively.

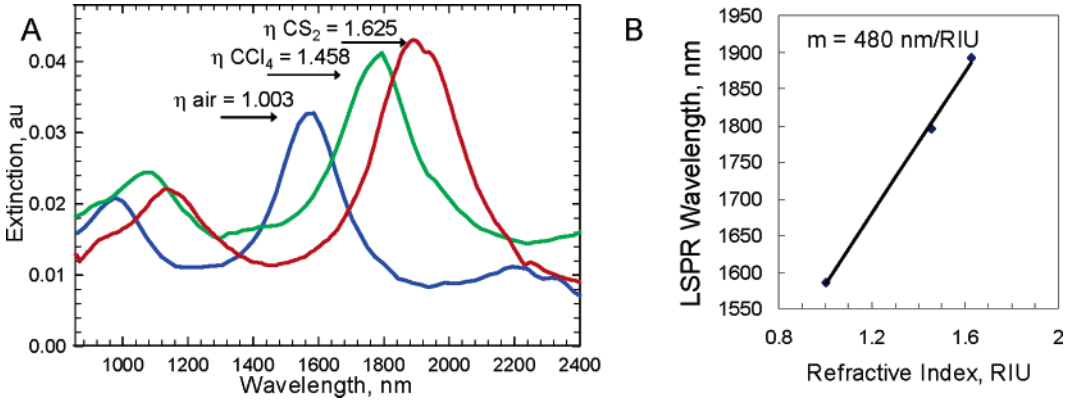

Figure 3. LSPR sensitivity to the local dielectric environment. (A) The LSPR extinction spectra for 194 nm diameter templated nanocrescents (height 34 nm) upon a change in dielectric environment. Refractive indices of each medium are shown near each longitudinal LSPR peak. (B) The LSPR for the nanocrescents is the sensitivity to dielectric environment is equal to the value of the slope.

Table 1. Representative LSPR Properties of Nanocrescents as a Function of Size and Aspect Ratio

diameter, nm	λ_{peak}, nm	E_{peak}, eV	sensitivity, nm/RIU	sensitivity, eV/RIU	relative sensitivity, %/RIU	fwhm, eV	FOM
410	2640[a]	0.47	879	0.14	29.5	0.07	2.0
	1570[b]	*0.79*	*440*	*0.21*	*25.6*	*0.13*	*1.6*
356[c]	2470	0.50	793	0.13	26.8	0.07	1.9
	1463	*0.85*	*416*	*0.21*	*26.2*	*0.13*	*1.6*
356[d]	2184	0.57	682	0.15	26.3	0.10	1.5
	1208	*1.03*	*459*	*0.32*	*31*	*0.26*	*1.4*
194[c]	1795	0.69	596	0.19	27.8	0.08	2.4
	1150	*1.08*	*418*	*0.31*	*28.4*	*0.20*	*1.6*
194[d]	1586	0.78	485	0.20	25.9	0.11	1.8
	978	*1.27*	*242*	*0.27*	*21.5*	*0.12*	*2.3*
125[c]	1305	0.95	416	0.25	26.8	0.21	1.2
125[d]	1083	1.14	368	0.32	28.2	0.32	1.0

[a] Values for longitudinal peaks are in normal font. [b] Values for transverse peaks are in italics. [c] Higher aspect ratio: incident angle = 40°. [d] Lower aspect ratio: incident angle = 20°. [e] Higher aspect ratio: thickness = 34 nm, incident angle = 20°. [f] Lower aspect ratio: thickness = 40 nm, incident angle = 20°.

transverse plasmon resonance peak (e.g., the peak at 1450 nm for 356 nm diameter crescents) is maximum when the incoming light is polarized parallel to the crescent's short axis. The sensitivity of the LSPR extinction peak amplitude to the incident light polarization with respect to the nanocrescent orientation is noticeably stronger for longitudinal peaks with decreases in peak amplitude of 300−500% with unfavorable polarization. In contrast, the transverse peak

amplitude varies by only 10−30% with a change in orientation with respect to the incident light polarization. Figure 2B shows the linear dependence of the LSPR peak wavelength for longitudinal and transverse peaks on the diameter of the PS template used to fabricate the crescents.

For some nanocrescents, a shoulder appears on the shorter wavelength side of the transverse peak as shown in Figure 2 for the 194, 356, and 465 nm diameter particles. The presence of a shoulder provides evidence that higher-order resonances also may contribute to the extinction spectra. In some cases, this shoulder may not be obvious and may contribute to the broadening of the transverse plasmon resonance peak. Table 1 lists full width at half-maximum (fwhm) values that can be used to compare peak broadening for different nanocrescents. For 125 nm diameter crescents, asymmetric rings, and even some low in-plane aspect ratio 194 nm diameter crescents, a single peak in the NIR was observed with a fwhm of 0.2−0.3 eV, at least twice as wide as the resonance peaks observed for well-separated longitudinal and transverse plasmon resonance peaks of 194 nm, 356 nm, and larger diameter crescents (i.e., fwhm of 0.08−0.12 eV). The increase in fwhm is likely due to the close proximity of the longitudinal and transverse LSPR peaks for the 125 nm diameter and low vertical aspect ratio 194 nm diameter crescents with small tip-to-tip distance. Decreases in tip-to-tip distance correlate with the convergence of transverse and longitudinal peaks and often a shoulder or a splitting of the main resonance peak in the NIR was observed. Calculations are being done to better understand the nature and contribution of the observed dipolar and potentially multipolar resonances to the extinction spectrum.

The number of plasmon resonance peaks observed in the spectra also is dependent on if the nanoparticle is a closed ring or an open crescent-shaped structure. Symmetrical rings are expected to have only two peaks: one peak corresponding to an out-of-plane resonance and a red-shifted peak due to the in-plane resonance. The location of the resonance depends on the ring dimensions as well as the aspect ratio. For example, rings with a 120 nm inner diameter/240 nm outer diameter exhibit a single peak in the NIR at 975 nm. The resonance peak location is similar to the 980 nm resonance wavelength reported for 92 nm inner-diameter/120 nm outer-diameter rings published by Aizpurua, et al.[28] Although the rings have different inner and outer radii, the heights are the nearly the same (i.e., 40−45 nm). The major structural difference between these nanorings is the in-plane aspect ratio which was 8.6 for the previously published rings, which is approximately twice the aspect ratio of 4 for the rings we fabricated. The similarity in the LSPR wavelengths for the two types of rings with different diameters indicates that the in-plane aspect ratio is as influential as the diameter of the rings on the resonance wavelength. We also have observed a sensitivity of the LSPR wavelength to the in-plane aspect ratio for nanocrescents with large tip-to-tip distances, as shown in Table 1. For example, as the deposition angle with respect to the source increased from 0° (Figure 1B) to 45° (Figure 1C), the crescents became more narrow and the in-plane aspect ratio increased accordingly. As a result, there was a consistent 13% red-shift in the longitudinal plasmon resonance peak for 194 nm diameter crescents (i.e., from 1585 to 1795 nm) and 356 nm diameter crescents (i.e., from 2184 to 2470 nm) as the in-plane aspect ratio increased. As shown in Table 1, the fwhm in eV decreases as the resonance energy decreases, so those peaks become more narrow as they red-shift.

Table 2. Extinction Properties of Gold Nanocrescents and Nanorings

diameter, nm	height, nm	extinction cross section, σ_{ext} x 10^4 nm^2	extinction efficiency, Q_{ext}
356[a]	37	71	23
194[a]	35	39	21
125[a]	26	57	21
125[b]	45	35	10

[a] Gold nanocrescents. [b] Gold nanorings.

Extinction is defined as $\epsilon = (1 - I/I_0)$ and is measured in transmission geometry using a spectrophotometer. The extinction cross section σ_{ext} was calculated as ϵ/N, where N is the particle density (particles/nm^2) estimated using SEM images. The extinction efficiency, Q_{ext}, is the ratio of the particle's σ_{ext} in nm^2 to the geometrical cross section (nm^2).[30] Representative σ_{ext} and Q_{ext} values are reported in Table 2. The extinction efficiencies are greater than 20 for the nanocrescents and exceed any value reported from experiments for nanostructures including rings,[28] discs,[30] and shells[31] by factors of 3−8. The experimentally measured extinction efficiencies also are greater than those calculated for rings ($Q_{ext} = 18$),[28] ellipsoids ($Q_{ext} = 13$),[32] and nanoshells ($Q_{ext} = 5$).[31] The Q_{ext} for the rings we fabricated was 10. This value lies between the experimental ($Q_{ext} = 8$) and calculated ($Q_{ext} = 18$) values published by Aizpurua, et al.[28] The large extinction efficiency is important for sensing applications because it is proportional to the spectroscopic signal-to-noise ratio and consequently should allow detection using fewer numbers of particles if all other parameters remain constant.

The sensitivity of the LSPR peaks to changes in the dielectric environment was investigated by collecting spectra of nanocrescents immobilized on glass surrounded by air, CCl_4, and CS_2. Representative spectra for 194 nm diameter nanocrescents are shown in Figure 3A, and sensitivity factors for several different nanocrescent samples are listed in Table 1. As evident from both the longitudinal and the transverse LSPR peaks, the nanocrescents are sensitive to the dielectric environment and the resonance peaks red-shift as the refractive index of the surrounding medium increases. This red-shift may be expressed as a change in the peak wavelength, $\Delta\lambda_{max}$, in nm or as a change in the peak energy, ΔE_{max}, in eV. The slope of the line in the inset graph of Figure 3B is the sensitivity factor for that nanocrescent sample.

The graphs in Figure 4A,B show the linear relationship between the measured sensitivity factors and the extinction spectra peak wavelengths for both longitudinal and transverse plasmon resonances. This linear relationship correlates with

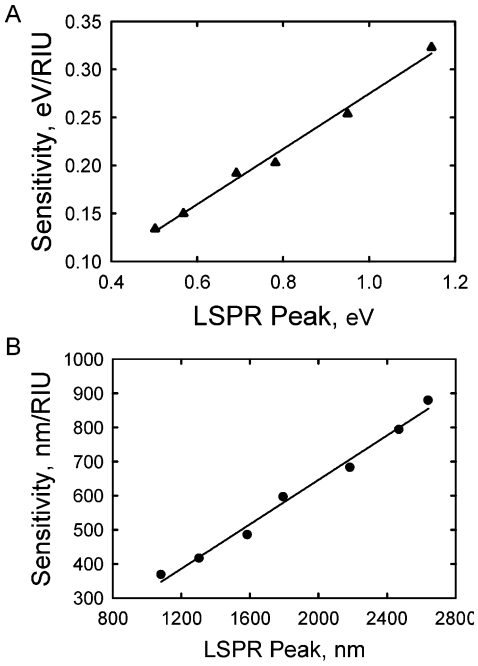

Figure 4. Nanocrescent LSPR sensitivities to dielectric environment. Sensitivity as a function of (A) LSPR wavelength and (B) energy for nanocrescents with different diameters. The slope of (B) defines the relative LSPR sensitivity in 1/RIU.

recent calculations by Miller and Lazarides.[33] Overall, the nanocrescents demonstrate a high sensitivity that increases with nanocrescent size and a red-shift of the LSPR wavelengths. Nanocrescents fabricated with 410 nm diameter PS templates had a sensitivity of 879 nm/RIU, greater than any other published experimental ensemble sensitivity factors, including those for nanorice (i.e., 801 nm/RIU).[34]

As shown in Figure 4, the sensitivity factor for nanocrescents follows two opposite trends as the size of the particle increases. The sensitivity in nm/RIU increases as recently predicted[33] and the sensitivity in eV/RIU decreases as the crescents become larger and the LSPR peaks red-shift. To reconcile these opposite tendencies and to express sensitivity in a way equally appropriate for small or large nanoparticles with LSPR peaks in the visible or infrared, we compare relative LSPR sensitivities. The relative LSPR sensitivity is the ratio of sensitivity in eV/RIU to the light energy in eV at the LSPR wavelength multiplied by 100%. As shown in Table 1, the relative sensitivity varies very little (i.e., within the uncertainty of peak wavelength measurements) for nanocrescents of different sizes with large openings. In contrast, there is an increase in sensitivity for the crescents with a small gap between crescent tips. Asymmetric rings have a slightly higher relative sensitivity (34%/RIU) than more open crescents (28%/RIU). The highest relative sensitivity of 38%/RIU was measured for 194 nm diameter crescents with a low out-of -plane aspect ratio (height 60−65 nm). We are probing the basis for this enhanced sensitivity.

The average relative sensitivities of the transverse peaks (27%/RIU) and the longitudinal peaks (27.5%/RIU) are statistically similar with higher standard deviation (3.6%/RIU) for transverse peaks than for longitudinal peaks (1.5%/RIU). The difference in the standard deviation may be explained by the smaller amplitude of the resonance peaks, resulting in a lower signal-to-noise ratio and a greater uncertainty in the exact peak position. We found no significant difference in relative sensitivity with changes in the orientation of the nanocrescents with respect to the electric field polarization of the incident light. Whether the incoming light was polarized along the longitudinal axis, the transverse axis, or between these two axes, the crescent's relative sensitivity remained approximately the same. In other words, the relative plasmon sensitivity of both the longitudinal and transverse peaks is independent of light polarization.

We calculated the relative sensitivities for other nanoparticles reported in literature using published data.[30−32,34−36] We found that the relative sensitivity from experimental measurements varies by at most a factor of 2, from the lowest relative sensitivity of 19%/RIU for 74 nm diameter, 20 nm high discs[30] to the highest relative sensitivity of 40%/RIU for 340 nm long, 80 nm diameter hematite−gold core−shells, or nanorice,[34] while the size (35−400 nm) and morphology of those particles are much more diverse. For example, 35 nm diameter silver spheres[36] have about the same relative sensitivity as 356 nm diameter gold nanocrescents (27−28%/RIU).

We calculated the sensing figure of merit (FOM) introduced by Van Duyne and co-workers.[37] The FOM is the ratio of LSPR sensitivity (eV/RIU) to fwhm (eV). Well-separated longitudinal and transverse LSPR peaks of 194, 356, and 410 nm diameter templated nanocrescents produced FOM values above 2, as shown in Table 1. The FOMs of rings and closed 194 nm diameter crescents are lower, in the range of 1.0−1.7, due to the merging of transverse and longitudinal LSPR peaks as discussed above. The largest FOM measured was 2.35 for 194 nm diameter templated open crescents. There are several single-particle measurements with FOMs greater than 3.[37−39] We calculated the FOM for several highly sensitive nanoparticles reported in literature using data from Sun, et al. (nanoshells, FOM 1.7),[31] Jensen, et al. (triangular prisms, FOM 1.7),[32] and Wang, et al. (nanorice, FOM 1),[34] and we found that nanocrescents have the highest ensemble FOM values reported in the literature.

In summary, gold nanocrescents exhibit unique and highly tunable LSPR properties, making them attractive for a number of surface-enhanced spectroscopy applications such as SERS and SEIRAS. Because of the high dielectric sensitivity (up to 880 nm/RIU), there is great potential for expanding the already broad spectral range by simply using a substrate with a higher dielectric constant such as silicon.[22] Characterization of the nanocrescents' near-field properties and the application of the particles in SEIRAS are underway.

Supporting Information Available: Experimental details, including materials, substrate preparation, fabrication, structural characterization, and spectroscopy measurements,

are described. This material is available free of charge via the Internet at http://pubs.acs.org.

References

(1) Kreibig, U.; Genzel, L. *Surf. Sci.* **1985**, *156*, 678−700.
(2) Mock, J. J.; Barbic, M.; Smith, D. R.; Schultz, D. A.; Schultz, S. *J. Chem. Phys.* **2002**, *116*, 6755−6759.
(3) Kreibig, U.; Vollmer, M. *Optical Properties of Metal Clusters*; Springer-Verlag: Berlin, 1995; Vol. 25.
(4) Haynes, C. L.; McFarland, A. D.; Zhao, L. L.; Van Duyne, R. P.; Schatz, G. C.; Gunnarsson, L.; Prikulis, J.; Kasemo, B.; Käll, M. *J. Phys. Chem. B* **2003**, *107*, 7337−7342.
(5) Sönnichsen, C.; Geier, S.; Hecker, N. E.; von Plessen, G.; Feldmann, J.; Ditlbacher, H.; Lamprecht, B.; Krenn, J. R.; Aussenegg, F. R.; Chan, V. Z. H.; Spatz, J. P.; Moller, M. *Appl. Phys. Lett.* **2000**, *77*, 2949−2951.
(6) Hutter, E.; Fendler, J. H. *Adv. Mater.* **2004**, *16*, 1685−1706.
(7) Campion, A.; Kambhampati, P. *Chem. Soc. Rev.* **1998**, *27*, 241−250.
(8) Haes, A. J.; Stuart, D. A.; Nie, S.; Van Duyne, R. P. *J. Fluoresc.* **2004**, *14*, 355−367.
(9) Lakowicz, J. R.; Geddes, C. D.; Gryczynski, I.; Malicka, J.; Gryczynski, Z.; Aslan, K.; Lukomska, J.; Matveeva, E.; Zhang, J. A.; Badugu, R.; Huang, J. *J. Fluoresc.* **2004**, *14*, 425−441.
(10) Sqalli, O.; Utke, I.; Hoffmann, P.; Marquis-Weible, F. *J. Appl. Phys.* **2002**, *92*, 1078−1083.
(11) Haes, A. J.; Van Duyne, R. P. *J. Am. Chem. Soc.* **2002**, *124*, 10596−10604.
(12) Reinhard, B. M.; Siu, M.; Agarwal, H.; Alivisatos, A. P.; Liphardt, J. *Nano Lett.* **2005**, *5*, 2246−2252.
(13) Nath, N.; Chilkoti, A. *Anal. Chem.* **2002**, *74*, 504−509.
(14) Elghanian, R.; Storhoff, J. J.; Mucic, R. C.; Letsinger, R. L.; Mirkin, C. A. *Science* **1997**, *277*, 1078−1081.
(15) Reynolds, R. A. I.; Mirkin, C. A.; Letsinger, R. L. *J. Am. Chem. Soc.* **2000**, *122*, 3795−3796.
(16) Shroff, H.; Reinhard, B. M.; Siu, M.; Agarwal, H.; Spakowitz, A.; Liphardt, J. *Nano Lett.* **2005**, *5*, 1509−1514.
(17) Penn, S. G.; He, L.; Natan, M. J. *Curr. Opin. Chem. Biol.* **2003**, *7*, 609−615.
(18) Liu, G. L.; Lu, Y.; Kim, J.; Doll, J. C.; Lee, L. P. *Adv. Mater.* **2005**, *17*, 2683−2688.
(19) Orendorff, C. J.; Gole, A.; Sau, T. K.; Murphy, C. J. *Anal. Chem.* **2005**, *77*, 3261−3266.
(20) Talley, C. E.; Jackson, J. B.; Oubre, C.; Grady, N. K.; Hollars, C. W.; Lane, S. M.; Huser, T. R.; Nordlander, P.; Halas, N. J. *Nano Lett.* **2005**, *5*, 1569−1574.
(21) McFarland, A. D.; Young, M. A.; Dieringer, J. A.; Van Duyne, R. P. *J. Phys. Chem. B* **2005**, *109*, 11279−11285.
(22) Jensen, T. R.; Van Duyne, R. P.; Johnson, S. A.; Maroni, V. A. *Appl. Spectrosc.* **2000**, *54*, 371−377.
(23) Fischer, U. C.; Zingsheim, H. P. *J. Vac. Sci. Technol.* **1981**, *19*, 881−885.
(24) Hulteen, J. C.; Van Duyne, R. P. *J. Vac. Sci. Technol., A* **1995**, *13*, 1553−1558.
(25) Love, J. C.; Gates, B. D.; Wolfe, D. B.; Paul, K. E.; Whitesides, G. M. *Nano Lett.* **2002**, *2*, 891−894.
(26) Charnay, C.; Lee, A.; Man, S. Q.; Moran, C. E.; Radloff, C.; Bradley, R. K.; Halas, N. J. *J. Phys. Chem. B* **2003**, *107*, 7327−7333.
(27) Lu, Y.; Liu, G. L.; Kim, J.; Mejia, Y. X.; Lee, L. P. *Nano Lett.* **2005**, *5*, 119−124.
(28) Aizpurua, J.; Hanarp, P.; Sutherland, D. S.; Käll, M.; Bryant, G. W.; de Abajo, F. J. G. *Phys. Rev. Lett.* **2003**, *90*.
(29) Shumaker-Parry, J. S.; Rochholz, H.; Kreiter, M. *Adv. Mater.* **2005**, *17*, 2131−2134.
(30) Hanarp, P.; Käll, M.; Sutherland, D. S. *J. Phys. Chem. B* **2003**, *107*, 5768−5772.
(31) Sun, Y. *Anal. Chem.* **2002**, *74*, 5297−5305.
(32) Jensen, T. R.; Duval, M. L.; Kelly, K. L.; Lazarides, A. A.; Schatz, G. C.; Van Duyne, R. P. *J. Phys. Chem. B* **1999**, *103*, 9846−9853.
(33) Miller, M. M.; Lazarides, A. A. *J. Phys. Chem. B* **2005**, *109*, 21556−21565.
(34) Wang, H.; Brandl, D. W.; Le, F.; Nordlander, P.; Halas, N. J. *Nano Lett.* **2006**, *6*, 827−832.
(35) Haes, A. J.; Van Duyne, R. P. *J. Am. Chem. Soc.* **2002**, *124*, 10596−10604.
(36) McFarland, A. D.; Van Duyne, R. P. *Nano Lett.* **2003**, *3*, 1057−1062.
(37) Sherry, L. J.; Chang, S. H.; Schatz, G. C.; Van Duyne, R. P.; Wiley, B. J.; Xia, Y. N. *Nano Lett.* **2005**, *5*, 2034−2038.
(38) Nehl, C. L.; Liao, H.; Hafner, J. H. *Nano Lett.* **2006**, *6*, 683−688.
(39) Sherry, L. J.; Rongchao, J.; Mirkin, C. A.; Schatz, G. C.; Van Duyne, R. P. *Nano Lett.* **2006**, *6*, 2060−2065.

NL062317O